A dynamic Fitting Method for Hybrid Time-Delayed and Uncertain Internally-Coupled Complex Networks: From Kuramoto Model to Neural Mass Model

Zhengyang Jin[1,2][0009-0008-8286-4246]

[1] University of Sussex, Brighton BN1 9RH, United Kingdom
zj69@sussex.ac.uk

[2] Institute for Infocomm Research (I2R), A*STAR, 138632, Singapore
JINZ0018@e.ntu.edu.sg

Abstract. The human brain, with its intricate network of neurons and synapses, remains one of the most complex systems to understand and model. The study presents a groundbreaking approach to understanding complex neural networks by introducing a dynamic fitting method for hybrid time-delayed and uncertain internally-coupled complex networks. Specifically, the research focuses on integrating a Neural Mass Model (NMM) called Jansen-Rit Model (JRM) with the Kuramoto model, by utilizing real human brain structural data from Diffusion Tensor Imaging (DTI), as well as functional data from Electroencephalography (EEG) and Magnetic Resonance Imaging (MRI), the study extends above two models into a more comprehensive brain-like model. This innovative multimodal model enables the simultaneous observation of frequency variations, synchronization states, and simulated electrophysiological activities, even in the presence of internal coupling and time delays. A parallel fast heuristics algorithm serves as the global optimization method, facilitating rapid convergence to a stable state that closely approximates real human brain dynamics. The findings offer a robust computational tool for neuroscience research, with the potential to simulate and understand a wide array of neurological conditions and cognitive states. This research not only advances our understanding of complex neural dynamics but also opens up exciting possibilities for future interdisciplinary studies by further refine or expand upon the current model.

Keywords: Complex Networks, Computational Neuroscience, Dynamic model fitting, Neural Mass Model, Kuramoto Model.

1 Introduction

The human brain stands as an intricate and dynamic network, comprised of billions of neurons interconnected by trillions of synapses. These neural components engage in complex electrochemical signaling mechanisms, orchestrating a symphony of interactions. This colossal and labyrinthine architecture is not merely responsible for rudimentary physiological functions such as respiration and cardiac rhythm; it also under-

pins advanced cognitive activities including memory, emotion, decision-making, and creative thought[1]. Consequently, the human brain can be conceptualized as a multi-layered, multi-scaled, and highly adaptive complex system. Its operational intricacies continue to pose some of the most formidable challenges in disciplines ranging from neuroscience to computational science [2].

Owing to the brain's staggering complexity and dynamic nature, scientists have been in relentless pursuit of effective models and methodologies to delineate and comprehend its operational mechanics. Among these, the Neural Mass Model (NMM) offers a valuable framework for investigating brain dynamics at macroscopic or mesoscopic scales [3]. This model simplifies the intricate web of interacting neurons into one or multiple 'neural masses,' thereby rendering the analysis of complex brain networks more tractable [4]. The NMM is particularly germane to the interpretation of neuroimaging data such as Electroencephalography (EEG) and Functional Magnetic Resonance Imaging (fMRI), as these modalities typically capture the collective activity of neuronal assemblies rather than the behavior of individual neurons [5]. Utilizing the Neural Mass Model enables researchers to gain deeper insights into fundamental characteristics of brain network dynamics, such as synchronization, rhythm generation, and information propagation [6]. However, it is worth noting that the model's reductive nature may limit its capacity to capture more nuanced neural activities or intricate network structures [7].

Concurrently, another pivotal framework for understanding brain network interactions is encapsulated in the concept of "Communication through Coherence" (CTC) [8]. In contrast to the Neural Mass Model, which primarily focuses on macroscopic electrical activities, CTC emphasizes the mechanisms by which neurons or neural masses achieve effective information transfer through coherent oscillatory activities [9]. Within this paradigm, coherent neural oscillations are posited as a conduit through which distantly located neural masses can transiently "lock" into specific phase relationships, thereby facilitating efficient information exchange. This coherence is not confined to oscillations at identical frequencies but can manifest across different frequency bands, engendering so-called "nested" oscillations. Such a multi-layered structure of coherence furnishes the brain with a flexible and efficient communication platform, enabling self-organization and adaptability across varying cognitive and behavioral states. Thus, CTC and the Neural Mass Model can be viewed as complementary tools, collectively illuminating the multifaceted dynamics of complex brain networks [10].

Worthy of mention in the same breath as models that describe coherence is the Kuramoto model, a mathematical construct frequently employed to describe the synchronization of large networks of oscillators [11]. This model employs a set of succinct differential equations to simulate the phase dynamics of oscillators, such as neurons or neural masses, thereby capturing synchronization phenomena within complex networks [12]. Numerous studies based on the Kuramoto model have ventured into exploring interactions between different brain regions and how these interactions

influence or reflect various cognitive states and functions [13, 14]. In synergy with CTC and the Neural Mass Model, the Kuramoto model offers a quantitative approach to assessing brain network coherence, particularly when considering network topology and oscillator interactions.

In the present study, we propose to integrate structural data extracted from real human brains, such as Diffusion Tensor Imaging (DTI), along with individual information data like Electroencephalography (EEG) and Magnetic Resonance Imaging (MRI), into the Neural Mass Model. This integration extends the model into a comprehensive Brain Mass Model (BMM) that accentuates its capacity to represent biophysical and physiological characteristics. The Jansen-Rit model is selected as the Neural Mass Model template to be applied on real human brain data, offering a mesoscopic description of physiological signals from neural clusters, as well as capturing influences from pathological conditions, pharmacological interventions, and external stimuli.

Furthermore, we employ the same real human brain structural data to augment the Kuramoto model, aligning its architecture with that of the BMM. This enables oscillator alignment at the network node level. We then attempt dynamic fitting of the extended Jansen-Rit model using the Kuramoto model, thereby facilitating simultaneous observation of mesoscopic electrophysiological signals and regional brain synchronization. In essence, this research enables multi-attribute observation of network states through dynamic fitting of complex systems, paving the way for simulating oscillatory coherence in the neural system following rhythmic or state changes. Given that both systems are mathematically expressed through differential equations—with the Kuramoto model outputting phase and the Jansen-Rit model outputting simulated local field potentials—the fitting process necessitates higher-order parameters. Considering the high-dimensional and non-convex nature of the task, parallel fast heuristics algorithms are chosen as the global optimization method.

Although the objective of this work is model fitting based on real data, it suffices to demonstrate that dynamic fitting of complex network systems can be applied to any potential models of the same category. It allows for the testing of multiple working states and attributes of the architecture under specific thematic data, while also enabling observation of structural changes in one model based on adjustments to the parameters of another. Lastly, we discuss the feasibility of applying this research to simulate the dynamics under various potential oscillatory states within neural systems, as well as the prospects for enhancing the accuracy and speed of the fitting process through the expansion of our original system.

2 Method

2.1 Real Human Brain Data Structure

In the present study, the estimation of structural brain networks was based on Diffusion Tensor Imaging (DTI) data, from Cabral's (2014) research [15]. All magnetic resonance scans were conducted on a 1.5 Tesla MRI scanner, utilizing a single-shot echo-planar imaging sequence to achieve comprehensive brain coverage and capture multiple non-linear diffusion gradient directions. To define the network nodes, the brain was parcellated into 90 distinct regions, guided by the Automated Anatomical Labeling (AAL) template [16]. Data preprocessing involved a series of corrections using the Fdt toolbox in the FSL software package ([26], FMRIB), aimed at rectifying image distortions induced by head motion and eddy currents. Probabilistic fiber tracking was executed using the probtrackx algorithm to estimate the fiber orientations within each voxel. For connectivity analysis, probabilistic tractography sampling was performed on fibers passing through each voxel [17]. This data served as the basis for both voxel-level and region-level analyses. Connectivity between different brain regions was ascertained by calculating the proportion of fibers traversing each region.

Ultimately, two 90x90 matrices, C_{ij} and D_{ij}, were generated (see Fig. 1). C_{ij} characterizes the connectivity and strength of connections between brain regions, whereas D_{ij} represents the communicative distance between them. To normalize these matrices, all off-diagonal elements were divided by their mean value, setting the mean to one. D_{ij} was also subjected to normalization to adapt to a discrete-time framework. This was accomplished by dividing D by the mean of all values greater than zero in the C matrix, followed by scaling through a simulated unit time and subsequent integer rounding for direct matrix indexing. (Estimation is carried out based on the Euclidean distance between the centroids of the segmented regions.[15])

2.2 Extended Neural Mass Model with Coupling Strength and Time Delay

Neural Mass Models (NMMs) serve as mesoscopic mathematical frameworks designed to capture the dynamic behavior of brain regions or neuronal assemblies. Unlike models that simulate the activity of individual neurons, NMMs aim to understand the integrated behavior of neural systems at a higher level of abstraction [3, 4, 5]. They typically employ a set of differential equations to describe the interactions between different types of neuronal populations, such as excitatory and inhibitory neurons, and their responses to external inputs. These models have found extensive applications in the analysis of neuroimaging data, including Electroencephalography (EEG) and Functional Magnetic Resonance Imaging (fMRI), as well as in simulating the dynamic expressions of neurological disorders like epilepsy and Parkinson's disease [18].

a

Barin Regions	Left	Right
Precentral	1	90
Frontal Sup	2	89
Front Sup Orb	3	88
Front Mid	4	87
Front Mid Orb	5	86
Front Inf Ope	6	85
Front Inf Tri	7	84
Front Inf Orb	8	83
Rolandic Oper	9	82
Supp Motor Ar	10	81
Olfactory	11	80
Front Sup Med	12	79
Front Med Orb	13	78
Rectus	14	77
Insula	15	76
Cingulum Ant	16	75
Cingulum Mid	17	74
Cingulum Post	18	73
Hippocampus	19	72
ParaHippocampal	20	71
Amygdala	21	70
Calcarine	22	69
Cuneus	23	68
Lingual	24	67
Occipital Sup	25	66
Occipital Mid	26	65
Occipital Inf	27	64
Fusiform	28	63
Postcentral	29	62
Parietal Sup	30	61
Parietal Inf	31	60
SupraMarginal	32	59
Angular	33	58
Precuneus	34	57
Paracentr Lobule	35	56
Caudate	36	55
Putamen	37	54
Pallidum	38	53
Thalamus	39	52
Heschl	40	51
Temporal Sup	41	50
Tempr Pole Sup	42	49
Temporal Mid	43	48
Tempr Pole Mid	44	47
Temporal Inf	45	46

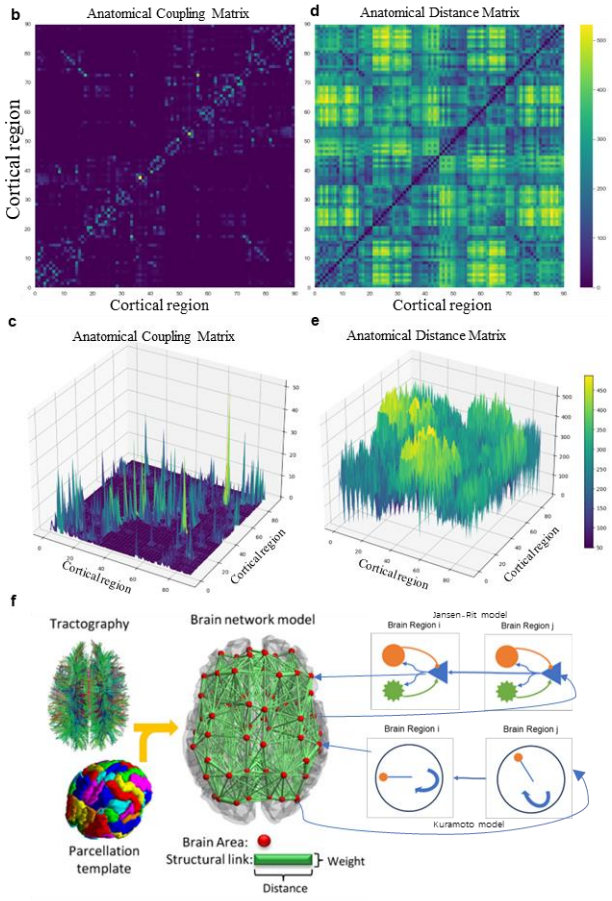

Fig. 1. Description of the real human brain structural template. (a) Indicates the brain region location corresponding to each node. (b) and (c) describe the coupling strength between brain regions, while (d) and (e) describe the time delays between them. (f) describes the virtual anatomical structure of the brain network model, as well as how each node is represented as either a Jansen-Rit model or a Kuramoto model.

One notable instantiation of NMMs is the Jansen-Rit Model (JRM), which has been frequently employed in past research to characterize specific large-scale brain rhythmic activities, such as Delta (1-4 Hz), Theta (4-8 Hz), and Alpha (8-12 Hz) waves. The JRM typically comprises three interconnected subsystems that represent pyramidal neurons, inhibitory interneurons, and excitatory interneurons. These subsystems are linked through a set of fixed connection weights and can receive one or multiple external inputs, often modeled as Gaussian white noise or specific stimulus signals. In previous research, the basic Jansen-Rit model has been extensively described, including structure, equations and parameter settings [19]. The JRM employs a set of nonlinear differential equations to describe the temporal evolution of the average mem-

brane potentials within each subsystem, their interactions, and their responses to external inputs.

In the present study, we extend the foundational single JRM to a network-level system comprising multiple JRMs. Each node in this network communicates based on the AAL brain structure data described in Section 2.1, and a more vivid depiction can be found in Fig 1. Given that local circuits are now expanded into large-scale, brain-like network circuits, nodes need to receive signals emitted from other nodes. This inter-node communication is governed by a parameter K_{ij}, which reflects the connectivity across areas. Additionally, considering the influence of inter-regional distances on signal transmission, the signals between nodes are also modulated by a parameter τ_{ij}, which represents the unit time required for a signal to reach a designated node. As a result, we can extend the original equations to accommodate these additional factors.

$$\begin{cases} \dot{y_0}^i(t) = {y_3}^i(t), \\ \dot{y_1}(t) = {y_4}^i(t), \\ \dot{y_2}(t) = {y_5}^i(t), \\ \dot{y_3}^i(t) = G_e\eta_e S\left[{y_1}^i(t) - {y_2}^i(t)\right] - 2\eta_e {y_3}^i(t) - {\eta_e}^2 {y_0}^i(t), \\ \dot{y_4}^i(t) = G_e\eta_e \left\{ p(t) + C_2 S\left[C_1 {y_0}^i(t)\right] + \sum_{j=1, j\neq i}^{N} K^{ij} x^j\left(t - \tau_D^{ij}\right) \right\} - 2\eta_e {y_4}^i(t) - {\eta_e}^2 {y_1}^i(t), \\ \dot{y_5}^i(t) = G_i\eta_i\{C_4 S\left[C_3 {y_0}^i(t)\right]\} - 2\eta_i {y_5}^i(t) - {\eta_i}^2 {y_2}^i(t). \end{cases}$$

2.3 Extended Kuramoto Model with Coupling Strength and Time Delay

The Kuramoto model serves as a mathematical framework for describing the collective behavior of coupled oscillators. Proposed by Yoshiki Kuramoto in 1975, the model aims to capture the spontaneous synchronization phenomena observed in groups of coupled oscillators [11]. In its basic form, the Kuramoto model describes N phase oscillators through the following set of ordinary differential equations:

$$\dot{\theta}_i = \omega_i + \frac{K}{N}\sum_{j=1}^{N} \sin\left(\theta_j - \theta_i\right)$$

Here, θ represents the phase of the oscillators, ω_i denotes the natural frequency of the i^{th} oscillator, N is the total number of oscillators, and K signifies the coupling strength between the oscillators. When the value of K is sufficiently low, it implies that the oscillators within the subsystem are in a weakly coupled state, operating more or less independently. As K increases and reaches a critical value K_c , the oscillators begin to exhibit synchronization. The coherence or order parameter of the Kuramoto model can be described using the following equation:

$$re^{i\psi} = \left|\frac{1}{N}\sum_{j=1}^{N} e^{i\theta_j}\right|$$

In this equation, $e^{i\theta_j}$ is a complex number with a modulus of 1. The value of r ranges from 0 to 1, with values closer to 1 indicating a more synchronized system. To adapt

the basic Kuramoto model to the current human brain network structure, the original equations can be reformulated as follows:

$$\dot{\theta}_\iota = \omega_i + K_{ij} \sum_{j=1}^{N} C_{ij} \sin\big(\theta_j(t - \tau_{ij}) - \theta_i(t)\big)$$

Given that the human brain network structure includes a matrix C_{ij} representing the connectivity between brain regions, the focus shifts to the influence between connectable network nodes. The global coupling parameter K is replaced by K_{ij}, eliminating the need for averaging. In this context, the emphasis is on detecting the coherence between two specific oscillators i and j, which can be calculated using the following equation within a time window T:

$$r = \left| \frac{1}{T} \int_0^T e^{i(\theta_i(t) - \theta_j(t - \tau_{ij}))}\, dt \right|$$

By adapting the Kuramoto model in this specialized context, the focus is shifted towards understanding the intricate relationships and synchronization phenomena between specific oscillators. This nuanced approach allows for the exploration of oscillator behavior in a more localized manner, contrasting with broader network models. It opens up avenues for investigating the subtleties of oscillator interactions, which could be particularly useful in specialized applications beyond the scope of traditional brain network models.

2.4 Dynamic Fitting for two extended model

As delineated in the preceding sections, the objective of this study is to dynamically fit the Jansen-Rit Model (JRM) and the Kuramoto model within the framework of the AAL human brain network structure. This integration aims to create a multimodal model that allows for the simultaneous observation of frequency variations, synchronization states, and simulated electrophysiological activities. Given that the JRM outputs time-varying electrical signals simulating membrane potentials, while the Kuramoto model outputs the phases of oscillators, a direct fitting of the outputs is not feasible. However, considering that both models yield time-varying signals, we can elevate them to a common output dimension by transforming their time-domain outputs into the frequency domain to obtain Power Spectrum Density (PSD).

For continuous-time signals $x(t)$, the PSD, $S(f)$, can be computed through Fourier Transform as follows:

$$S(f) = \lim_{\mathrm{T}\to\infty} \frac{1}{T} \left| \int_{-T/2}^{T/2} x(t)\, e^{-i2\pi f \mathrm{t}} dt \right|^2$$

In our specific case, dealing with discrete signals, we employ a window with a range equal to the maximum value of the delay matrix and calculate the PSD using the periodogram method:

$$PSD[k] = \frac{1}{N} \left| FFT(x[n] - \frac{1}{N} \sum_{j=1}^{N-1} x[n]) \right|^2$$

Here, FFT denotes the Fast Fourier Transform, and the input to the function is the signal with its DC component removed. The modulus is then squared and normalized.

Our optimization strategy synergistically combines the inherent attributes of the models with the characteristics of their operational states, employing a segmented parameter-fitting approach. Given the operational rules of the Kuramoto model, the natural frequencies often have a significant influence in the system's initial state. Therefore, during the fitting process, we use the difference between the x-axis mappings of the peak PSD values of the two models as the initial loss. This initial loss serves as a guiding metric until the PSD peaks of both models closely align in the frequency domain. Subsequently, we proceed to the next phase of parameter adjustment. Given the varying connectivity across nodes, the coupling strength will determine the overall energy levels. Accordingly, the coupling strength K for each node is adjusted based on the current PSD differences; in other words, the height of the peak dictates the direction of K's development. In our practical implementation, considering that the JRM operates under resting parameters and includes Gaussian white noise as input, we have opted not to introduce specific stimuli to simulate conditions the human brain might encounter. Therefore, we have not extended our segmented, multimodal parameter-fitting approach to include environment-sensitive adaptive state-switching, which would automatically select the parameters to be fitted based on changes in network states.

3 Results

In this investigation, an initial imperative step involved meticulous parameter optimization for the Jansen-Rit Model (JRM). Given the plethora of tunable parameters inherent to the JRM and our aspiration to operate the model under a unified parameter configuration, this optimization was quintessential. After exhaustive testing and calibration, we ascertained optimal values for several pivotal parameters to engender optimal outputs within the Alpha rhythm spectrum. Specifically, the Average Excitatory Synaptic Gain (A) was determined to be 3.25mV, the Average Inhibitory Synaptic Gain (B) was 22mV, the Average Synapse Number (C) was 135, and the Firing Threshold (PSP or v0) was 5.52mV.

Moreover, we scrutinized overarching resolution parameters that influence the model's operation, including the Coupling Gain (G) =10 and Mean Velocity (v) = 25m/s. As depicted in Fig 2, an optimal parameter configuration was identified to ensure the output remains ensconced within the Alpha rhythm domain.

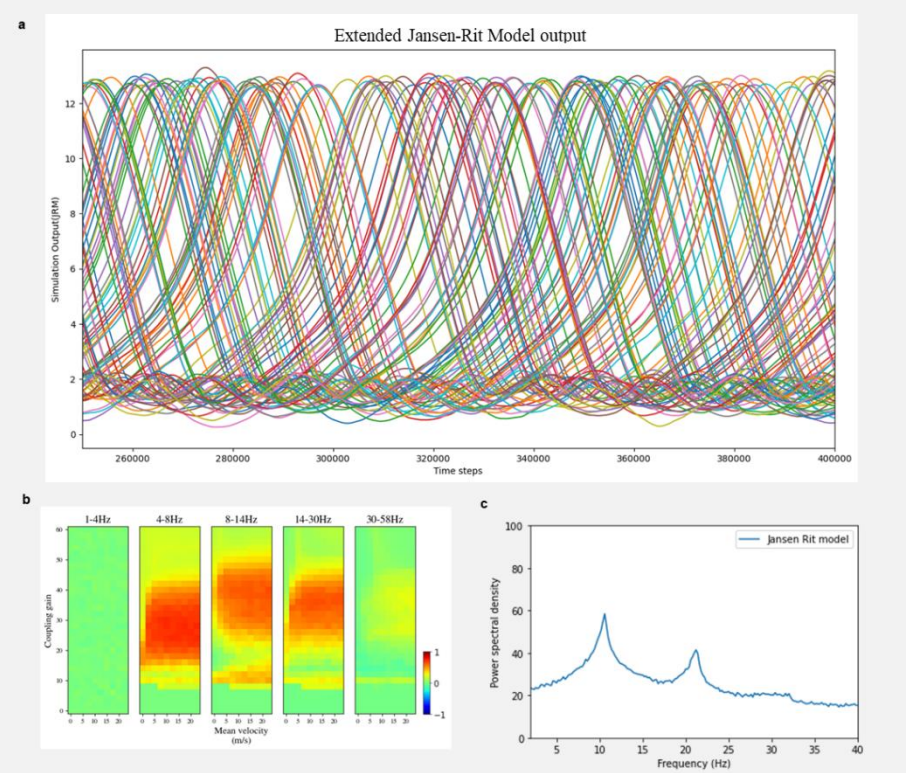

Fig. 2. Exploration of the system output for the Extended Jansen-Rit model. (a) Shows the output of the JRM in 90 brain regions (extracted from a window of 250,000 to 400,000 time units). (b) Displays the correlation maps between the underlying structural connectivity matrix and the FC matrices extracted from all combinations of model parameters, for different frequency bands [19]. (c) Presents the overall PSD (Power Spectral Density) of the model at this stage.

Upon the foundation of these optimized parameters, the system was initialized and executed, culminating in a stable output state as evidenced in the simulation results (see Figure 3.). Since our Kuramoto model uses a consistent direction simulation, the x-axis coordinate can be used to determine the current operating frequency of most oscillators. Intriguingly, due to the intricate interplay of complex connections and parameters, certain nodes exhibited conspicuously elevated frequencies compared to others. Concurrently, a subset of relatively quiescent nodes manifested diminished activity ranges, contrasting starkly with nodes subjected to copious stimulation. These observations not only corroborate the model's heterogeneity and complexity but also allude to the potential for further refinement through parameter scaling.

Subsequently, we embarked on dynamic fitting of the steady-state JRM using the Kuramoto model. Astonishingly, the congruence between the two models, as gauged through Power Spectrum Density (PSD), was attained expeditiously within just 80

fitting segments. Initially, the natural frequencies of the Kuramoto model manifested multiple peaks across a 5-100Hz range in the PSD. However, as the preliminary fitting phase approached culmination, the Kuramoto model was observed to have transitioned into a frequency operation phase that was substantially congruent with that of the JRM. Specifically, after 70 fitting segments, the PSD curve closely approximated the target state of the JRM, and the loss descent curve plateaued, indicating that the system had reached a proximate operational state.

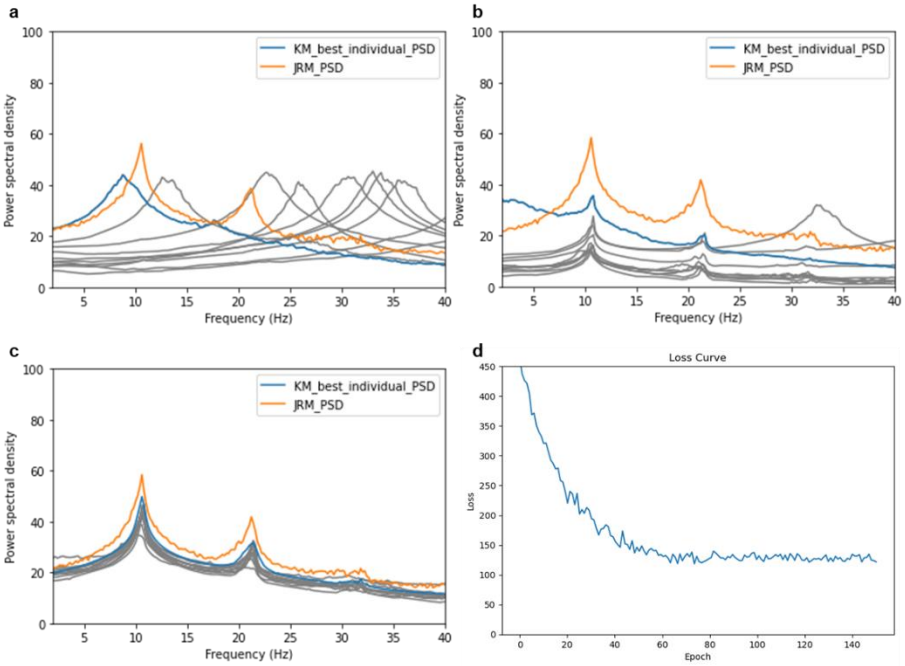

Fig. 3. The fitting process of the Power Spectrum and the decline curve of the loss. (a) represents the parameter initialization stage, (b) marks the end of the first fitting stage, (c) indicates when the fitting stage reaches a steady state, and (d) shows the loss curve which represent the difference of two models' PSD.

4 Discussion

This study delves into a method for dynamic fitting of multimodal complex systems, aimed to dynamically fit the Jansen-Rit Model (JRM) and the Kuramoto model within the framework of the Automated Anatomical Labeling (AAL) human brain network structure. Our results indicate that the optimized parameters for the JRM were effective in simulating Alpha rhythms, and the Kuramoto model was able to rapidly adapt to the JRM's steady-state output. Our findings corroborate previous studies that have employed the JRM and Kuramoto models separately to understand brain dynamics [15, 19]. However, our work extends the existing literature by integrating these two

models, thereby offering a more comprehensive tool for understanding complex neural dynamics.

The successful integration of the JRM and Kuramoto models suggests that it is feasible to create a multimodal model for the simultaneous observation of frequency variations, synchronization states, and simulated electrophysiological activities. This could pave the way for more nuanced models that can better capture the multifaceted nature of brain dynamics. The ability to dynamically fitting has significant implications for neuroscience research, potentially offering a robust computational tool for simulating and understanding various neurological conditions or cognitive states. This could be particularly beneficial for the development of targeted therapeutic interventions.

One salient limitation of our study resides in the utilization of standardized parameter settings for the JRM, which may not fully encompass the extensive spectrum of neural dynamics. Future investigations could delve into the ramifications of parameter variations. Moreover, our research did not incorporate specific stimuli to emulate conditions that the human brain might encounter, leaving room for future exploration in this domain. For instance, the introduction of simulations for conditions such as epilepsy [21], Parkinson's disease [22], Attention Deficit Hyperactivity Disorder (ADHD) [23], and cognitive function assessments [24] could be particularly enlightening. On another front, achieving higher fidelity in model fitting remains an imperative research objective. Given the rich output waveforms generated by the JRM, it would be myopic to confine ourselves to standard Kuramoto oscillators. The incorporation of limiters within the oscillators emerges as a promising avenue worth exploring. Alternatively, we could contemplate expanding each node into a fully connected—or otherwise interconnected—multi-oscillator Kuramoto sub-network, thereby potentially enriching the system's output [25]. In this manner, the utilization of dual complex systems to study specific neural activities becomes feasible. Not only does this allow for the analysis of synchronization phenomena under such activities, but it also enables a multi-faceted examination that could yield more comprehensive insights.

References

1. Sporns, O. (2011) Networks of the brain. Cambridge, Mass: MIT Press.
2. Jirsa, V.K. and Haken, H. (1996) ‘Field theory of electromagnetic brain activity’, Physical Review Letters, 77(5), pp. 960–963.
3. Deco, G., Jirsa, V.K. and McIntosh, A.R. (2011) ‘Emerging concepts for the dynamical organization of resting-state activity in the brain’, Nature Reviews Neuroscience.
4. David, O. and Friston, K.J. (2003) ‘A neural mass model for MEG/EEG’: NeuroImage, 20(3), pp. 1743–1755.
5. Friston, K.J. (2009) ‘Modalities, modes, and models in functional neuroimaging’, Science, 326(5951), pp. 399–403.
6. Breakspear, M. (2017) ‘Dynamic models of large-scale brain activity’, Nature Neuroscience, 20(3), pp. 340–352.

7. Deco, G., Jirsa, V.K. and McIntosh, A.R. (2011) ‘Emerging concepts for the dynamical organization of resting-state activity in the brain’, Nature Reviews Neuroscience.
8. Fries, P. (2005). A mechanism for cognitive dynamics: neuronal communication through neuronal coherence. Trends in cognitive sciences, 9(10), 474-480.
9. Fries, P. (2015). Rhythms for Cognition: Communication through Coherence. Neuron, 88(1), 220-235.
10. Canolty, R. T., & Knight, R. T. (2010). The functional role of cross-frequency coupling. Trends in cognitive sciences, 14(11), 506-515.
11. Kuramoto, Y. (1975). Self-entrainment of a population of coupled non-linear oscillators. In International Symposium on Mathematical Problems in Theoretical Physics (pp. 420-422). Springer, Berlin, Heidelberg.
12. Strogatz, S. H. (2000). From Kuramoto to Crawford: exploring the onset of synchronization in populations of coupled oscillators. Physica D: Nonlinear Phenomena, 143(1-4), 1-20.
13. Cabral, J., Hugues, E., Sporns, O., & Deco, G. (2011). Role of local network oscillations in resting-state functional connectivity. NeuroImage, 57(1), 130-139.
14. Deco, G., Jirsa, V. K., & McIntosh, A. R. (2011). Emerging concepts for the dynamical organization of resting-state activity in the brain. Nature Reviews Neuroscience, 12(1).
15. Cabral, J. *et al.* (2014) ‘Exploring mechanisms of spontaneous functional connectivity in MEG: How delayed network interactions lead to structured amplitude envelopes of band-pass filtered oscillations’, *NeuroImage*, 90, pp. 423–435.
16. Tzourio-Mazoyer, N. *et al.* (2002) ‘Automated anatomical labeling of activations in spm using a macroscopic anatomical parcellation of the mni mri single-subject brain’, *NeuroImage*, 15(1), pp. 273–289.
17. Behrens, T.E.J. *et al.* (2007) ‘Probabilistic diffusion tractography with multiple fibre orientations: What can we gain?’, *NeuroImage*, 34(1), pp. 144–155.
18. Wendling, F. *et al.* (2002) ‘Epileptic fast activity can be explained by a model of impaired GABAergic dendritic inhibition: Epileptic activity explained by dendritic dis-inhibition’, *European Journal of Neuroscience*, 15(9), pp. 1499–1508.
19. Sanchez-Todo, R. *et al.* (2018) ‘Personalization of hybrid brain models from neuroimaging and electrophysiology data’. bioRxiv.
20. Spiegler, A. *et al.* (2016) ‘Selective activation of resting-state networks following focal stimulation in a connectome-based network model of the human brain’, *eNeuro*.
21. Jirsa, V.K. *et al.* (2014) ‘On the nature of seizure dynamics’, *Brain*, 137(8).
22. Rubin, J.E. and Terman, D. (2004) ‘High frequency stimulation of the subthalamic nucleus eliminates pathological thalamic rhythmicity in a computational model’, *Journal of Computational Neuroscience*, 16(3), pp. 211–235.
23. Castellanos, F.X. and Proal, E. (2012) ‘Large-scale brain systems in ADHD: beyond the prefrontal–striatal model’, *Trends in Cognitive Sciences*, 16(1), pp. 17–26.
24. Deco, G. and Kringelbach, M.L. (2014) ‘Great expectations: using whole-brain computational connectomics for understanding neuropsychiatric disorders’, *Neuron*, 84(5).
25. Bauer, L.G. *et al.* (2022) ‘Quantification of kuramoto coupling between intrinsic brain networks applied to fmri data in major depressive disorder’, *Frontiers in Computational Neuroscience*, 16.
26. Smith, S.M. *et al.* (2004) ‘Advances in functional and structural MR image analysis and implementation as FSL’, *NeuroImage*, 23, pp. S208–S219. https://fsl.fmrib.ox.ac.uk/fsl/fslwiki